COMPOSITION AND STRUCTURAL STATE OF COLUMBITE – TANTALITE FROM THE HARDING PEGMATITE, TAOS COUNTY, NEW MEXICO

GREGORY R. LUMPKIN[1]

*Materials Division, Australian Nuclear Science and Technology Organisation, Private Mail Bag 1,
Menai, New South Wales 2234, Australia*

ABSTRACT

Columbite – tantalite is an important accessory mineral in the Harding granitic pegmatite, a subhorizontal, zoned, complex spodumene-type pegmatite emplaced within the Proterozoic Vadito Group in northern New Mexico. Columbite – tantalite is most abundant in the beryl (wall) zones of the pegmatite, with lesser quantities in the interior units. Average compositions of 25 samples plotted in the columbite quadrilateral form a distinct trend halfway along the $MnNb_2O_6$ – $MnTa_2O_6$ join, defined by $0.25 < Ta/(Ta + Nb) < 0.57$ and $0.91 < Mn/(Mn + Fe) < 0.99$. Internal fractionation is evident in the $Ta/(Ta + Nb)$ value which, on average, increases from 0.38 in the beryl zones to 0.49 in the interior lithologic units. The average $Mn/(Mn + Fe)$ value increases only slightly from 0.95 in the beryl zones to 0.98 in the interior units. These variations are accompanied by minor decreases in the average amounts of W, Ti, and U. The structural state of columbite – tantalite from the Harding pegmatite is bimodal. Samples from the beryl zone are highly disordered to partially ordered (f between 0.11 and 0.62, Q between 0.16 and 0.66), but samples from interior units are highly ordered (f between 0.97 and 1.02, Q between 0.87 and 0.93). The XRD and TEM results indicate that most partially ordered samples represent a simple transition between disordered and ordered distributions of cations; for example, there are no stacking faults or unusual superstructures. However, one highly disordered specimen may contain micrometer-scale domains and nanometer-scale intergrowths of completely disordered ($f = Q = 0$) and partially ordered ($f = Q = 0.2$) columbite. Possible factors causing the observed trend in structural state include a decrease in cooling rate by as much as two to three orders of magnitude and the presence of minor elements. The average U content of most samples is <0.5 wt.% UO_2, thus restricting the accumulated radiation damage to a low level. Some radiation damage is documented by HRTEM in local regions of the sample containing 0.4 to 0.8 wt.% UO_2.

Keywords: columbite – tantalite, cation ordering, cooling models, domain structures, fractionation, radiation damage, Harding granitic pegmatite, New Mexico.

SOMMAIRE

La columbite – tantalite s'avère un minéral accessoire important dans la pegmatite granitique de Harding, qui forme un massif subhorizontal zoné, de type complexe à spodumène, mis en place dans un encaissant protérozoïque du Groupe de Vadito, dans le nord du Nouveau-Mexique. Cet accessoire est le plus abondant dans les zones externes à béryl de la pegmatite, et nettement moins abondant dans les zones internes. La composition moyenne de 25 échantillons est présentée dans le quadrilatère de la columbite; ils forment un tracé distinct à mi-chemin le long de la série $MnNb_2O_6$ – $MnTa_2O_6$, dans les intervalles $0.25 < Ta/(Ta + Nb) < 0.57$ et $0.91 < Mn/(Mn + Fe) < 0.99$. Le fractionnement interne du système est évident d'après la valeur du paramètre $Ta/(Ta + Nb)$, qui augmente, en moyenne, de 0.38 dans les zones à béryl jusqu'à 0.49 dans les zones internes. La valeur moyenne de $Mn/(Mn + Fe)$ n'augmente que légèrement, de 0.95 dans les zones à béryl jusqu'à 0.98 dans les zones internes. Ces variations sont accompagnées de légères diminutions dans la teneur moyenne en W, Ti, et U. Le degré d'ordre de la columbite – tantalite à Harding est bimodal. Les échantillons de la zone à béryl sont fortement désordonnés ou partiellement ordonnés (f entre 0.11 et 0.62, Q entre 0.16 et 0.66), mais ceux qui proviennent des zones internes sont fortement ordonnés (f entre 0.97 et 1.02, Q entre 0.87 et 0.93). Les données de diffraction X et de microscopie électronique par transmission montrent que dans la plupart des cas, les échantillons partiellement ordonnés représentent une simple transition entre une distribution désordonnée et une distribution ordonnée des cations. Il ne semble pas y avoir de défauts d'empilement ou de surstructures inattendues. En revanche, un échantillon fortement désordonné pourrait contenir des domaines micrométriques et des intercroissances nanométriques de columbite complètement désordonnée ($f = Q = 0$) et partiellement ordonnée ($f = Q = 0.2$). Parmi les facteurs qui pourraient expliquer le comportement observé du degré d'ordre figurent une diminution du taux de refroidissement, possiblement de deux ou trois ordres de grandeur, et la présence d'éléments mineurs. La teneur moyenne des échantillons en uranium est inférieure à 0.5% de UO_2 (en poids), ce qui limite l'endommagement du réseau cristallin. Le dommage semble plus élevé, selon les observations par microscopie électronique par transmission à haute résolution, dans des régions locales contenant entre 0.4 et 0.8% de UO_2.

(Traduit par la Rédaction)

Mots-clés: columbite – tantalite, mise en ordre des cations, modèles de refroidissement, structures en domaines, fractionnement, endommagement du réseau dû à la radiation, pegmatite granitique de Harding, Nouveau-Mexique.

[1] *E-mail address*: grl@nucleus.ansto.gov.au

INTRODUCTION

Members of the columbite – tantalite group of orthorhombic AB_2O_6 oxides are the predominant Nb–Ta minerals found in granites, pegmatitic granites, and granitic pegmatites of the rare-element class (Černý 1989a, b). Columbite – tantalite is rarely eclipsed as the major Nb–Ta oxide phase, for example, by wodginite and microlite in the Tanco pegmatite at Bernic Lake, Manitoba (Ercit 1986) and by microlite in the Harding pegmatite, New Mexico (Jahns & Ewing 1976). Most columbite – tantalite compositions can be adequately represented within the columbite – tantalite quadrilateral defined by the end-members $FeNb_2O_6$, $FeTa_2O_6$, $MnNb_2O_6$, and $MnTa_2O_6$. Recent investigations have shown that compositional variations are related to the overall level of chemical differentiation of a given body of pegmatite, plus internal fractionation represented dramatically by the sequence of lithologic units present. In general, columbite – tantalite compositions exhibit enrichment in Mn and Ta with progressive fractionation of granitic-pegmatite-forming melt – fluid systems (Černý et al. 1985, Černý & Ercit 1985, 1989, Černý 1989a, b, Spilde & Shearer 1992, Von Knorring & Fadipe 1981).

The structural state of columbite – tantalite is defined by the distribution of Mn + Fe and Nb + Ta over the available octahedrally coordinated sites in space group *Pbcn*. In the disordered structure, the cations are randomly distributed over the $4c$ and $8d$ sites, resulting in a unit cell with an a cell dimension of approximately 4.8 Å. Ordering of Mn + Fe on $4c$ and Nb + Ta on $8d$ results in an ...*ABBABB*... site population sequence on (100) and consequent tripling of the a axis to approximately 14.4 Å (Sturdivant 1930, Nickel et al. 1963). In addition to compositional variation, the structural state of columbite – tantalite varies considerably, ranging from completely disordered to highly ordered. Most specimens tend to have an intermediate degree of cation ordering (Černý & Ercit 1985, 1989, Ercit et al. 1995). Factors that control the order – disorder process are poorly understood, but it appears that the presence of minor elements, overall size of the pegmatite body, and location of the sample within the body (*e.g.*, wall zone *versus* core) all have an effect on the degree of cation order.

The presence of radioactivity in columbite – tantalite is well established; however, in many examples, this property is due to inclusions or alteration by another phase with a relatively high U or Th content (Heinrich 1962, Lumpkin 1992). Effects of radiation damage on the columbite structure have received very little attention, with one analytical electron microscope study appearing in the recent literature (Lumpkin 1992). Studies of suites of different radioactive minerals from a given locality provide important information on element partitioning, radiation-damage effects, and processes of geochemical alteration. Such information

is directly applicable to an assessment of the long-term performance of crystalline nuclear waste forms (*e.g.*, Ewing et al. 1988).

This study was initiated to investigate the chemical composition, degree of cation order, and radiation-damage effects in columbite – tantalite from the Harding pegmatite. The results and discussion are based on combined results of electron-microprobe analyses, X-ray diffraction work, and transmission electron microscopy of 25 samples. Owing to the limited number of samples large enough for X-ray powder diffraction, the chemical aspects of this study are limited to a brief description of the major chemical variations related to internal fractionation of the pegmatite system.

LOCATION AND GENERAL GEOLOGY

The Harding pegmatite is located in Taos County, New Mexico, approximately 10 km east of Dixon, within the southern part of the Picuris range. Host rocks at this locality are highly deformed metavolcanic, metavolcaniclastic, and metapelitic schists of the Vadito Group. These rocks have an age of approximately 1700 Ma. Metapelitic units of the Vadito Group contain large porphyroblasts of andalusite, cordierite, and staurolite, which indicate maximum metamorphic conditions of 300 to 400 MPa and 550°C. The Harding pegmatite has an age of 1300 ± 50 Ma and postdates major F_1 and F_2 folding and peak metamorphic conditions, which occurred at approximately 1400 Ma. The main body of the pegmatite is roughly tabular, dips to the south at 10°, and has maximum known dimensions of $30 \times 100 \times 400$ m. Exposures of the main body occur primarily between amphibolite on the hanging wall and quartz – mica schists on the footwall. The pegmatite crystallized during isobaric cooling from 650°C to ~550°C or lower at a pressure of 330–350 MPa. Hydrothermal processes continued to ~350°C, and were followed by uplift and cooling [see Chakoumakos & Lumpkin (1990) for details and a review].

A vertical succession of lithologic units characteristic of the Harding pegmatite in the area of the main quarry is shown in Figure 1. These units have been described in great detail elsewhere (Jahns & Ewing 1976, Lumpkin et al. 1986, Chakoumakos & Lumpkin 1990), and will only be summarized here. The uppermost unit is known as the *upper beryl zone*, a continuous unit consisting of quartz + albite–oligoclase + muscovite ± microcline. Six of the samples used in this investigation were collected from the upper beryl zone near the east and west ends of the main quarry. One of these samples comes from a small pegmatite offshoot into the hanging-wall amphibolite. Throughout most of the main quarry, the upper beryl zone is underlain by the *quartz zone*, a semi-continuous unit of massive quartz ± albite ± muscovite that is generally poor in rare-element accessory minerals.
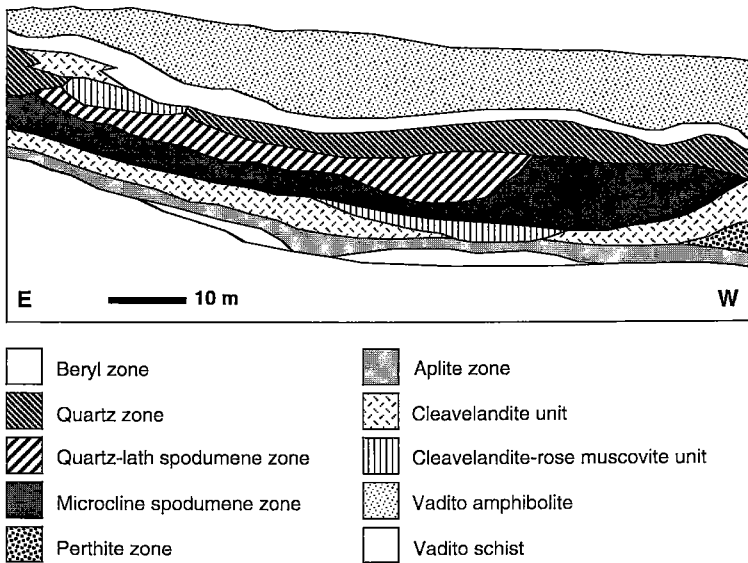
FIG. 1. East–west cross section of the Harding pegmatite in the area of the main quarry. The main units of the wall zones are the beryl, quartz, and aplite zones. The core of the pegmatite is dominated by the quartz – lath spodumene and microcline – spodumene zones in this area. Adapted from Jahns & Ewing (1976).

Below the quartz zone is a discontinuous core unit of spodumene + quartz ± albite ± microcline ± muscovite ± lepidolite known as the *quartz – lath spodumene zone,* a unit famous for its giant crystals of spodumene (Jahns & Ewing 1976, Chakoumakos & Lumpkin 1990). Much of the core of the Harding pegmatite is occupied by the *microcline – spodumene zone,* a semicontinuous unit composed of microcline + spodumene + quartz ± albite ± muscovite with local gradations into nearly pure masses of lepidolite. The *"cleavelandite" unit* consists of albite + quartz ± muscovite and forms a discontinuous layer mainly beneath the microcline – spodumene zone, but also occurs locally at higher levels between this unit and the quartz zone and as patches within the beryl zone. Although columbite – tantalite occurs in all three of these units, microlite is the dominant Nb–Ta oxide mineral in the interior zones of the Harding pegmatite. Four columbite – tantalite samples from these units were large enough for X-ray powder-diffraction work.

A continuous *aplite zone* forms much of the lowermost section of the pegmatite and also occurs as patches within other units. This unit consists of fine-grained albite + quartz ± muscovite ± lepidolite,

with accessory apatite. Parts of the footwall are comprised of the *lower beryl zone,* a discontinuous, mineralogical equivalent of the upper beryl zone. Beryl and columbite – tantalite are the major accessory minerals of the lower beryl zone. Fifteen of the columbite – tantalite samples used in this study were collected from the lower beryl zone near the summit of North Knob, where excellent exposures of the "cleavelandite" unit, aplite zone, and lower beryl zone occur in an up-dip projection of the Harding pegmatite north of the main quarry (see Jahns & Ewing 1976).

The remaining lithologic units of the Harding pegmatite are the *blocky perthite zone* occurring in the western part of the main body, the *"cleavelandite" – rose muscovite unit,* which replaces part of the quartz – lath spodumene zone and microcline – spodumene zone (Fig. 1), and the *lepidolite – "cleavelandite" unit,* which is found primarily in the thin eastward extensions of the pegmatite. Rare-element accessory minerals are uncommon in the blocky perthite zone and "cleavelandite" – rose muscovite unit. Minor amounts of microlite, columbite – tantalite, and rare grains of fersmite have been found in the lepidolite – "cleavelandite" unit, but these are generally too small for X-ray diffraction work.

X-ray-diffraction analysis

Powder X-ray-diffraction (XRD) profiles of 25 samples were obtained using an automated Scintag diffractometer operated at 40 kV and 30 mA. Samples were scanned from 10 to 80°2θ at a scan rate of 0.5° per minute using graphite-monochromatized Cu$K\alpha$ radiation. Peak positions were refined using Scintag deconvolution software and corrected using BaF$_2$ as an internal standard. Unit-cell parameters were refined in space group *Pbcn*, based on the ordered supercell, by the method of least squares using the procedure developed by Appleman & Evans (1973). For proper indexing of diffraction patterns, calculated peak positions and intensities were generated using FINAX software for a hypothetical columbite – tantalite having the composition MnNbTaO$_6$ and five different cation distributions described by $f = Q = 0, 0.25, 0.50, 0.75,$ and 1.00 (definitions of f and Q and method of calculation are given below). Cell parameters for each of these cation distributions were estimated from the *a–c* plot of Wise *et al.* (1985).

Electron-microprobe analysis

Polished sections were examined using a JEOL 733 Superprobe operated with an accelerating potential of 15 kV, 20 nA sample current, and a focussed probe diameter of 1 μm. Each element was counted for 40 seconds or until a standard deviation of 0.5% was reached. Raw data were corrected for deadtime, drift, and reduced to weight percent oxides using the empirical procedures developed by Bence & Albee (1968). The following standards were employed: manganotantalite (Mn,Ta), olivine (Mg,Fe), cassiterite (Sn), benitoite (Ti), stibiotantalite (Sb,Bi), UO$_2$ (U), YPO$_4$ (Y), LaPO$_4$ (La), CePO$_4$ (Ce), NdPO$_4$ (Nd), SmPO$_4$ (Sm), CaWO$_4$ (Ca,W), and NaNbO$_3$ (Nb). A set of empirical overlap-factors were employed to correct for interference problems, particularly those for Ta–W, La–Ce, La–Nd, and Ce–Sm peak overlaps.

Transmission electron microscopy

Crushed grains of selected samples were dispersed in acetone and collected on copper grids supported by holey carbon films. Specimens were examined using a JEOL 2000FX transmission electron microscope (TEM) operated at 200 kV. Standard techniques of diffraction, bright field, and high-resolution imaging were employed. High-resolution (HRTEM) images were recorded at a magnification of 410,000 to 500,000 using axial illumination, 120 μm C2 condenser lens aperture, 50 μm objective lens aperture, and objective lens defocus values between –60 and –120 nm. Selected-area diffraction patterns were taken in the [010] or [001] orientations using a double-tilt (± 30°) specimen holder, 100 μm field-limiting aperture, and a camera length of 83 cm. A Gatan heating stage with double tilting capability was used for *in situ* heating experiments. Electron-diffraction patterns of selected grains were recorded before and after heating at 300, 500, 750, and 1000°C for 2 hours at each temperature. Sample compositions were checked by analytical electron microscopy (AEM) using a Tracor–Northern energy-dispersion X-ray detector equipped with a 7.6 μm Be window. This detector is interfaced to a Link ISIS X-ray analyzer. Individual spectra were acquired for 300 seconds at a count rate of 600 to 800 cps, ~25% deadtime, emission current of 115 μA, and current density of ~2 pA/cm^2. Peak counts were obtained using the Link ISIS software package TEMQuant, which employs digital filtering to suppress the background, a least-squares fitting procedure, and a library of reference spectra. Element concentrations were calculated using the Cliff–Lorimer ratio method and a set of experimentally determined k-factors [see Lumpkin *et al.* (1994) for further details].

Chemical composition

Average electron-microprobe analyses of the Harding columbite – tantalite samples reveal major oxide contents of 25 to 51 wt.% Nb$_2$O$_5$, 29 to 57 wt.% Ta$_2$O$_5$, 15 to 17 wt.% MnO, and only 0.2 to 1.6 wt.% FeO. The amounts of other elements present are minor. Maximum amounts of 0.8 wt.% WO$_3$, 1.2 wt.% TiO$_2$, and 0.8 wt.% UO$_2$, 0.2 wt.% Y$_2$O$_3$, 0.2 wt.% Ln$_2$O$_3$, and 0.2 wt.% CaO are typical of the Harding specimens [Suchomel (1976) reported WO$_3$ contents up to 2.9 wt.%, possibly owing to uncorrected interference with Ta]. Results of the analyses also showed that Mg, Al, Sc, Sb, Sn, Pb, and Bi are routinely near or below the 0.1 wt.% level. Structural formulae, calculated on the basis of 6.00 oxygen atoms per formula unit, indicate that near ideal AB_2O_6 stoichiometry is approached in all of the samples. Major-element contents are 0.89 to 0.99 Mn, 0.01 to 0.09 Fe, 0.8 to 1.5 Nb, and 0.5 to 1.2 Ta atoms per formula unit. Minor elements have maximum levels approaching 0.03 W, 0.06 Ti, 0.02 U, and 0.01 Y, Ln, and Ca atoms per formula unit. A summary of the average major-element proportions and minor-element contents is given in Table 1.

Major-element compositions of the Harding samples are plotted in the columbite – tantalite quadrilateral shown in Figure 2a. Compositions form a distinct linear trend approximately halfway along the MnNb$_2$O$_6$ – MnTa$_2$O$_6$ join defined by Ta/(Ta + Nb) between 0.25 and 0.57 and Mn/(Mn + Fe) between 0.91 and 0.99, with a positive correlation between Mn and Ta. The average compositions of the columbite – tantalite are given by lithologic unit in Table 2 and indicate that

the linear trend is due in part to differentiation of the Harding pegmatite-forming magma. With increasing fractionation from wall zones to interior units, the ratio Ta/(Ta + Nb) increases from a minimum of 0.33 to 0.49. In comparison, Mn/(Mn + Fe) increases only slightly, from 0.94 to 0.98. These fractionation-related changes are accompanied by a decrease in the average amounts of W, Ti, and U (see Table 2). From the available data, the average amounts of the rare-earth elements (*REE* = lanthanides + Y) in the Harding samples did not change significantly with increasing fractionation.

Structural state

Results of the cell-parameter refinements are given in Table 3 and plotted in the *a–c* diagram (*cf.* Wise *et al.* 1985) shown in Figure 2b. The data points scatter along the Mn-rich side of the figure, ranging from highly disordered to highly ordered. Furthermore, there is a bimodal distribution of data points corresponding to specimens from the beryl zone and specimens from the interior lithologic units. Samples from the beryl zone constitute the highly disordered to partially ordered group, whereas samples from the interior units are highly ordered. In order to characterize the cation distributions in greater detail, a parameter defined as the fractional degree of order, *f*, was calculated from the observed cell parameters using a slightly modified version of equation 6 given by Ercit *et al.* (1995):

$$f = [1727 - 941.6(c - 0.2329a)]/100$$

where $f = 0$ for a disordered distribution of cations and $f = 1$ for a fully ordered arrangement. Because this equation is based directly on the topology of the *a–c* plot and does not account for the presence of minor elements, the alternative approach of Ercit *et al.* (1995) was used to estimate the degree of order, *Q*, from the observed cell parameters and average compositions of the samples:

$$Q = 1 - (|h|/0.166)$$

$$|h| = [(a_u - a_H)^2 + (b_u - b_H)^2 + (c_u - c_H)^2]^{1/2}$$

and

$$a_H = 14.258 + 0.166Mn/(Mn + Fe) + 0.0072Ta/(Ta + Nb) - 0.015Ti - 0.005Sn + 0.013Sc$$

$$b_H = 5.7296 + 0.031Mn/(Mn + Fe) + 0.0024Ta/(Ta + Nb) - 0.006Ti - 0.002Sn + 0.005Sc$$

$$c_H = 5.0495 + 0.033Mn/(Mn + Fe) + 0.011Ta/(Ta + Nb) - 0.001Ti$$

where $Q = 0$ for a disordered distribution of cations and $Q = 1$ for an ordered distribution. The parameter $|h|$

TABLE I. SUMMARY OF AVERAGE COMPOSITIONS OF COLUMBITE-TANTALITE FROM THE HARDING PEGMATITE

	$\frac{Ta}{Ta+Nb}$	$\frac{Mn}{Mn+Fe}$	W pfu	Ti pfu	U pfu	REEs pfu
CT1	0.390	0.960	0.005	0.036	0.003	0.000
CT2	0.459	0.982	0.000	0.005	0.000	0.007
CT2a	0.492	0.988	0.002	0.011	0.000	0.009
CT13	0.436	0.970	0.007	0.052	0.005	0.007
CT14	0.510	0.977	0.000	0.000	0.000	0.006
CT14a	0.506	0.976	0.003	0.002	0.000	0.006
CT15	0.349	0.955	0.007	0.040	0.001	0.012
CT16	0.424	0.971	0.009	0.056	0.000	0.012
CT17	0.351	0.961	0.012	0.035	0.003	0.000
CT18	0.439	0.975	0.011	0.044	0.005	0.006
CT21	0.436	0.976	0.009	0.047	0.005	0.009
CT22	0.569	0.988	0.004	0.011	0.002	0.000
CT23	0.511	0.970	0.006	0.032	0.006	0.007
CT24	0.270	0.919	0.007	0.029	0.001	0.002
CT25	0.416	0.959	0.005	0.041	0.005	0.003
CT28	0.547	0.980	0.004	0.020	0.002	0.008
CT29	0.407	0.959	0.007	0.046	0.006	0.002
CT30	0.456	0.961	0.007	0.022	0.002	0.006
CT38	0.477	0.965	0.008	0.049	0.012	0.002
CT39	0.435	0.963	0.009	0.054	0.012	0.005
CT45	0.283	0.918	0.005	0.027	0.000	0.003
CT46	0.277	0.942	0.005	0.039	0.002	0.006
CT50	0.258	0.912	0.008	0.031	0.002	0.003
CT52	0.371	0.967	0.010	0.033	0.003	0.001
CT55	0.413	0.962	0.006	0.047	0.005	0.004

represents the magnitude of the heating vector in direct space, and a_u, b_u, and c_u are the observed cell parameters for an unheated sample. The values of a_H, b_H, and c_H are calculated parameters for a fully ordered distribution of cations after heating [see Ercit *et al.* (1995) for further details]. Here, the coefficients for Ti, Sn, and Sc have been modified for concentrations given in atoms per formula unit.

Cation distributions estimated by the two methods given above are listed in Table 3. Results of the calculations show that *f* is between 0.11 and 0.62 for samples from the beryl zone, and between 0.97 and 1.02 for samples from the interior lithologic units. Using the *f* values as a guide, the latter group of samples appear to be fully ordered. In comparison, *Q* is between 0.16 and 0.66 for samples from the beryl zone, and between 0.87 and 0.93 for samples from the interior zones. The *Q* values indicate that the bimodal distribution in *a–c* space is due in part to sample composition and the presence of minor elements. Furthermore, samples that appear to be fully ordered in *a–c* space are only about 90% ordered after correcting for the effects of composition. Differences between the two sets of calculations are, however, small relative to the estimated error of ±0.05 for *f* (Černý & Ercit 1989) and ±0.08 for *Q* when calculated values of a_H, b_H, and c_H are used (Ercit *et al.* 1995).

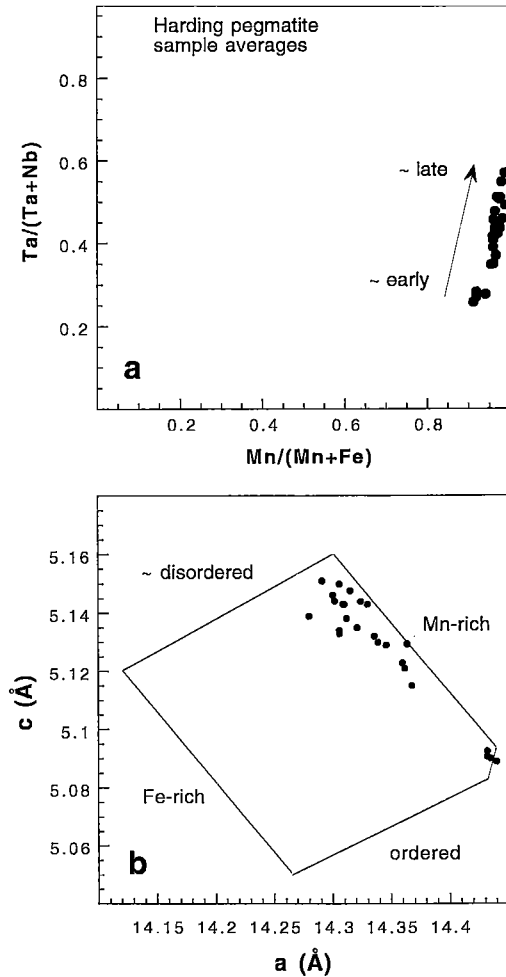Four samples covering the full range of cation order were investigated further using a combination

TABLE 2. AVERAGE COMPOSITIONS OF COLUMBITE-TANTALITE FROM THE BERYL ZONE AND INTERIOR ZONES OF THE HARDING PEGMATITE

	Upper beryl zone		Interior zones		Lower beryl zone	
	mean	$1\sigma_{n-1}$	mean	$1\sigma_{n-1}$	mean	$1\sigma_{n-1}$
Ta/(Ta+Nb)	0.33	0.06	0.49	0.02	0.43	0.07
Mn/(Mn+Fe)	0.94	0.02	0.981	0.005	0.96	0.01
W *	0.007	0.002	< 0.002		0.007	0.002
Ti	0.035	0.007	0.005	0.003	0.04	0.01
Sn	< 0.003		< 0.003		< 0.003	
U	0.003	0.002	< 0.001		0.004	0.003
Sc	< 0.003		< 0.003		< 0.003	
REEs	0.002	0.001	0.007	0.002	0.004	0.003

* Minor element contents given in atoms per formula unit

patterns of completely disordered grains show no evidence of diffraction maxima due to a superstructure and can be indexed on the disordered subcell with $a \approx 4.8$ Å (cf. Figs. 3a, b). Electron-diffraction patterns of samples CT55, CT30, and CT14 all exhibit superlattice diffraction maxima (e.g., $h = 2, 4$) and can be indexed on the ordered supercell, with $a \approx 14.4$ Å (Figs. 4b, c, d). Although sensitive to the effects of dynamic scattering, the electron-diffraction patterns are qualitatively consistent with the XRD results and exhibit increasing relative intensities of superlattice

FIG. 2. Average compositions and unit-cell parameters of columbite – tantalite from the Harding pegmatite. a) Compositions plotted in the columbite quadrilateral. Note approximate fractionation trend from Nb-rich to Ta-rich compositions. b) Unit-cell parameters plotted in the a–c diagram of Wise *et al.* (1985). Disordered and partially ordered samples are from the upper and lower beryl (wall) zones. Ordered samples are from interior units.

of electron diffraction and high-resolution imaging. Zone-axis electron-diffraction patterns were taken in orientations with $h = 0$ in order to observe the effects of differences in structural state. Figure 3 shows [010] diffraction patterns and (h02) intensity profiles of representative grains of samples CT18, CT55, CT30, and CT14. The highly disordered sample, CT18, gave selected-area diffraction patterns indicating a mixture of completely disordered and partially ordered columbite – tantalite. The [010] zone-axis electron-diffraction

TABLE 3. UNIT-CELL DIMENSIONS AND ESTIMATES OF CATION ORDER IN COLUMBITE-TANTALITE FROM THE HARDING PEGMATITE

|	a (Å)	b (Å)	c (Å)	V (Å³)	f	Q
CT1	14.312(2)	5.7576(7)	5.1381(7)	423.63(7)	0.28	0.32
CT2	14.435(3)	5.775(1)	5.090(1)	424.3(1)	1.00	0.89
CT2a	14.432(2)	5.7651(7)	5.0907(7)	423.56(6)	0.99	0.93
CT13	14.309(4)	5.758(1)	5.143(1)	423.7(1)	0.22	0.30
CT14	14.440(2)	5.7763(8)	5.089(1)	424.47(8)	1.02	0.87
CT14a	14.432(2)	5.7657(9)	5.0925(8)	423.76(8)	0.97	0.93
CT15	14.302(2)	5.7553(8)	5.1441(8)	423.42(7)	0.20	0.25
CT16	14.300(3)	5.759(1)	5.1462(8)	423.8(1)	0.17	0.25
CT17	14.330(5)	5.760(1)	5.143(2)	424.5(2)	0.27	0.40
CT18	14.291(1)	5.759(1)	5.151(1)	423.9(1)	0.11	0.17
CT21	14.306(2)	5.756(1)	5.1499(9)	424.07(8)	0.15	0.25
CT22	14.364(2)	5.7650(6)	5.1295(8)	424.77(7)	0.47	0.56
CT23	14.346(3)	5.7642(6)	5.129(1)	424.13(8)	0.44	0.51
CT24	14.339(3)	5.7595(9)	5.130(1)	423.66(9)	0.41	0.51
CT25	14.306(2)	5.7522(8)	5.1329(6)	422.39(7)	0.31	0.31
CT28	14.360(3)	5.766(1)	5.123(1)	424.2(1)	0.52	0.58
CT29	14.310(3)	5.7602(8)	5.143(1)	423.93(8)	0.23	0.31
CT30	14.368(5)	5.759(2)	5.115(2)	423.2(2)	0.62	0.66
CT38	14.336(3)	5.7651(8)	5.132(1)	424.15(9)	0.39	0.47
CT39	14.315(2)	5.7642(6)	5.1476(8)	424.75(7)	0.19	0.32
CT45	14.321(3)	5.761(1)	5.135(1)	423.7(1)	0.32	0.40
CT46	14.280(4)	5.743(1)	5.139(1)	421.4(1)	0.20	0.16
CT50	14.362(3)	5.762(1)	5.121(1)	423.8(1)	0.55	0.65
CT52	14.324(2)	5.757(1)	5.144(1)	424.15(8)	0.25	0.36
CT55	14.306(3)	5.754(2)	5.134(1)	422.6(1)	0.30	0.31
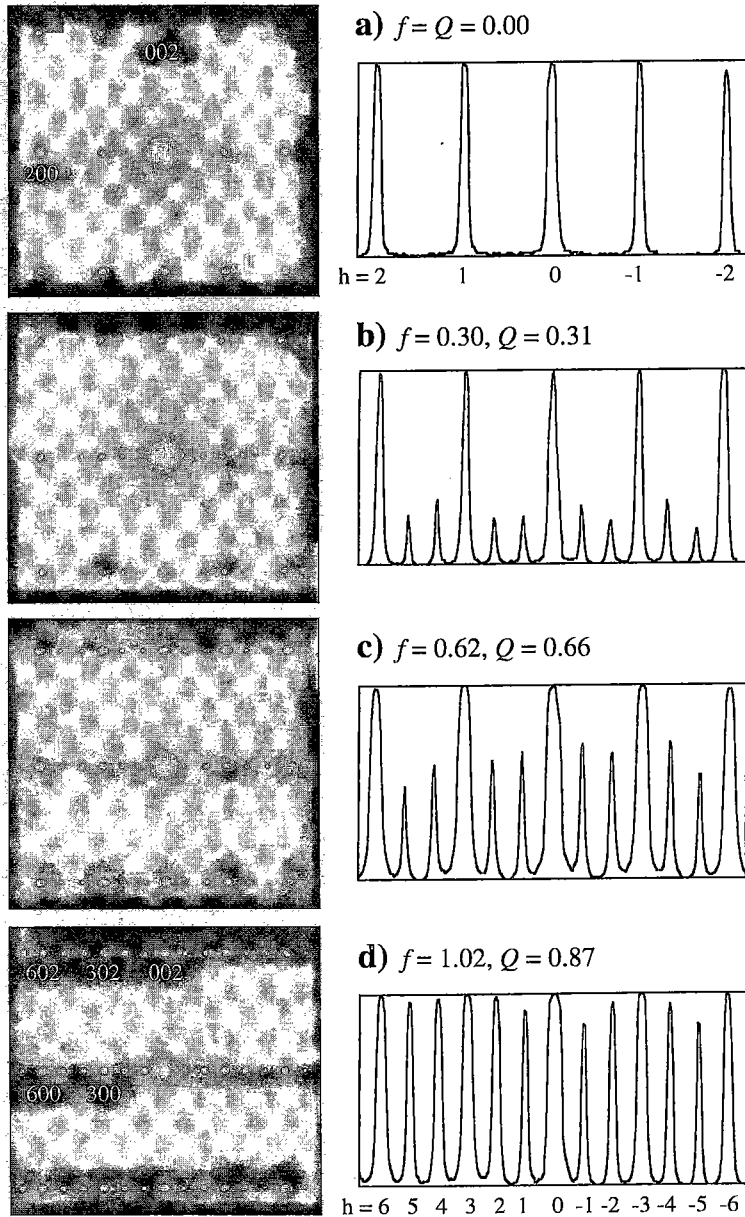
FIG. 3. Electron-diffraction patterns and corresponding (h02) intensity profiles of selected samples of columbite – tantalite. a) Disordered domain of sample CT18. Note the absence of superlattice diffraction maxima and indexing based on the disordered subcell. b) Partially ordered sample CT55. Note the presence of superlattice diffraction maxima and indexing based on the ordered cell. c) Partially ordered sample CT30. d) Highly ordered sample CT14. [010] zone axis.
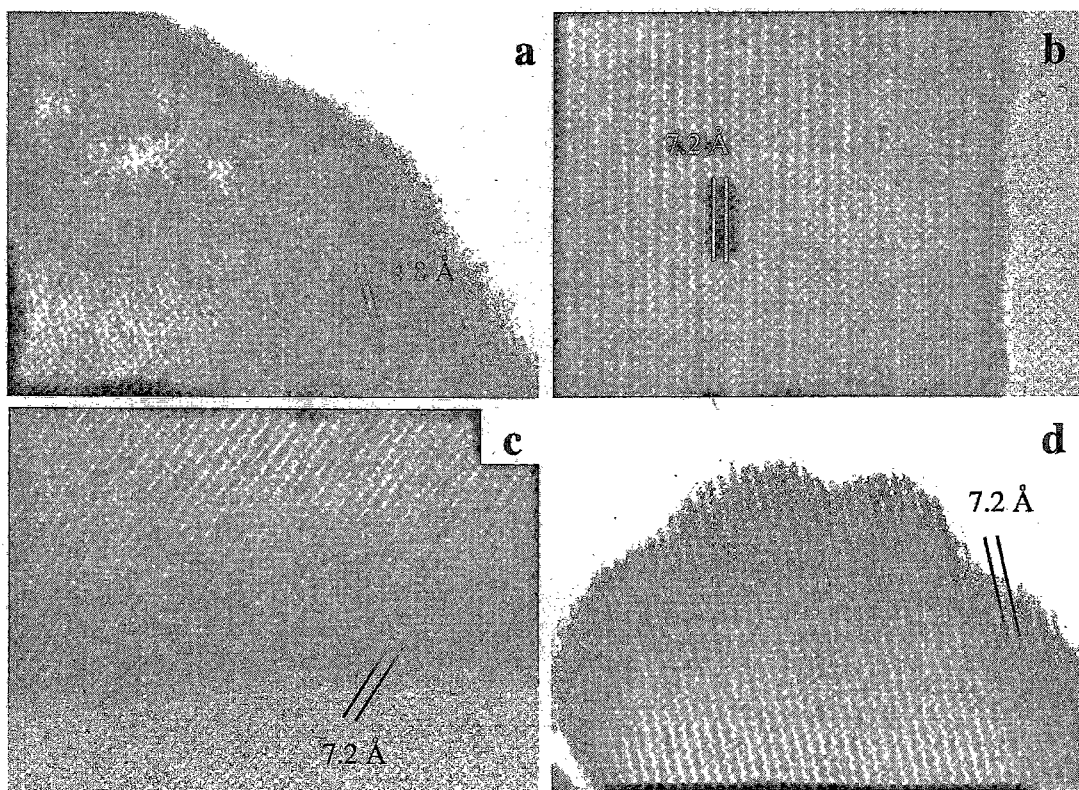
FIG. 4. HRTEM images of the same samples as shown in Figure 4. a) Sample CT18 showing 4.8 Å (100) subcell lattice fringes. b) Partially ordered sample CT55, c) partially ordered sample CT30, and d) highly ordered sample CT14, all showing 7.2 Å (200) supercell lattice fringes. Note the level of crystallographic perfection and lack of intergrowths on (100).

reflections with increasing values of f and Q. Note that for the [010] orientation, the kinematically forbidden $(h00)$ reflections with $h = 2n + 1$ occur as a result of multiple diffraction.

Representative HRTEM images of the same four samples are shown in Figure 4. Completely disordered areas of sample CT18 exhibit lattice fringes of the 4.8 Å (100) subcell when imaged in the [010] orientation (Fig. 5a). In comparison, the two partially ordered (CT55, CT30) samples and one highly ordered sample (CT14) generally show continuous lattice fringes of the 7.2 Å (200) supercell for the conditions of thickness and defocus used in this study (Figs. 4b, c, d). Some grains may exhibit 3.6 Å (400) lattice fringes in relatively thin areas, and the 14.4 Å (100) repeat commonly is observed in thicker areas, but there is no evidence for stacking disorder or higher-order superstructures on the (100) plane. As noted above, both disordered and partially ordered grains were found in sample CT18. The actual size of the domains in this instance must be greater than the minimum grain-size of ~0.5 μm. The

[001] zone-axis electron-diffraction patterns of two examples are shown in Figure 5. The disordered grain is indexed on the 4.8 Å subcell (Fig. 5a), whereas the partially ordered grain has weak diffraction spots that can be indexed on the 14.4 Å supercell (Fig. 5b). Notice that in this orientation, there are no kinematically forbidden reflections that arise from multiple diffraction. On the basis of a linear comparison of the intensities of the diffracted beams and cation distributions in the four samples, the partially ordered domains of CT18 are estimated to have local values of $f = Q = 0.2$. As expected, these values are higher than the bulk XRD values, $f = 0.11$ and $Q = 0.17$.

HRTEM images of sample CT18 also suggest that there are regions within the crystal where small domains of disordered and partially ordered structural state coexist. One of these regions is shown in Figure 5c, where the domains appear as separate areas with and without lattice fringes on a scale as small as 5–10 nm. The possibility that these could be tilt-related domains was tested and discarded. Tilting the specimen
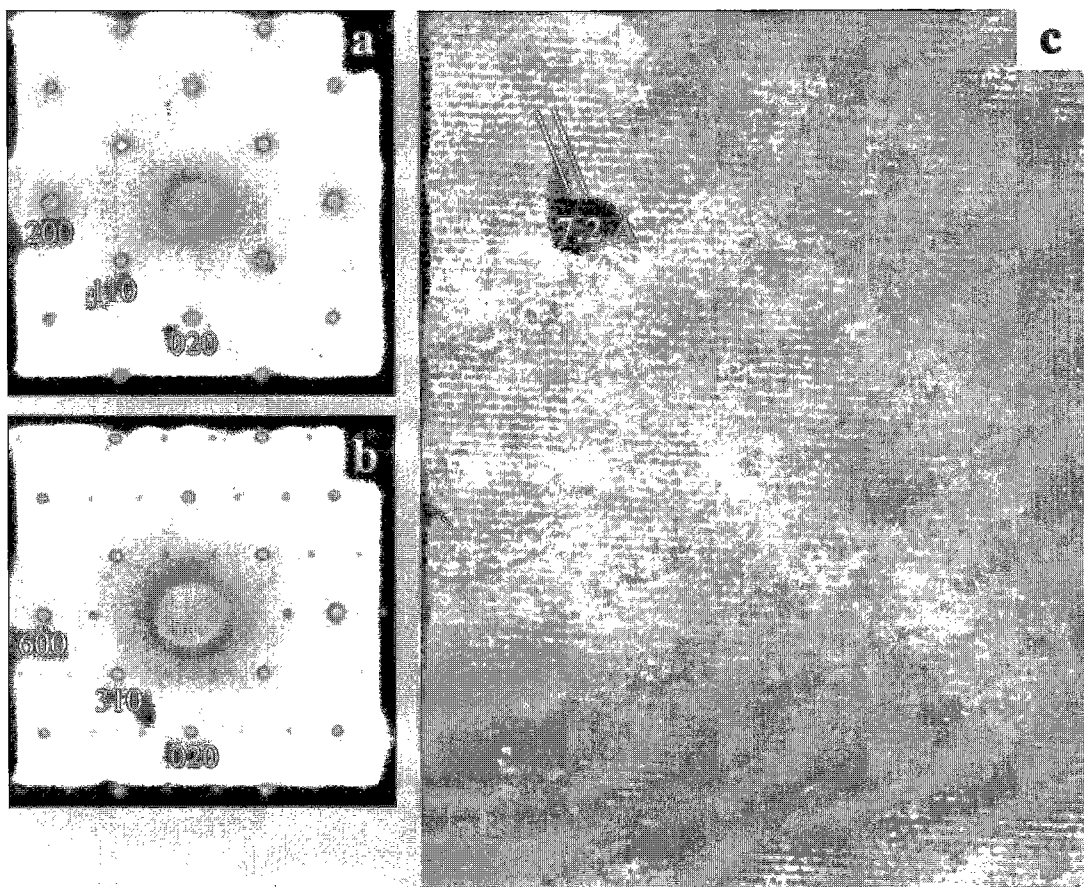
FIG. 5. Electron-diffraction patterns and HRTEM images illustrating the occurrence of disordered and partially ordered domains in sample CT18. a) Electron-diffraction pattern of the [001] zone of a disordered grain. b) Electron-diffraction pattern of the [001] zone of a partially ordered grain. Note that in this orientation, there are no reflections due to multiple diffraction. c) HRTEM image showing a fine-scale intergrowth of disordered and partially ordered domains.

failed to produce lattice fringes in the areas that appear to be disordered. The absence of lattice fringes in disordered domains imaged down [001] can be explained by the absence of diffracted beams attributed to the 4.8 Å (100) subcell in this orientation, combined with the objective lens aperture, which excludes all other diffracted beams with spacings of less than ~3 Å. A second possibility is that the domains are due to radiation damage; however, the U content of this region was checked by AEM and found to be too low (<0.2 wt.% UO_2) to have caused the observed microstructure.

Heating experiments

Several micrometric grains of sample CT18 were selected for heating experiments carried out *in situ*

in the electron microscope using a heating stage. The experiments were designed to test whether or not changes in cation ordering could be detected over the temperature range of 300 to 1000°C. Results are shown in Figures 6 and 7 for two representative cases, one a completely disordered grain and the other a partially ordered grain. For the relatively short heating times used in these experiments, the results indicate that there is essentially no development of cation ordering for the disordered grains at temperatures up to 750°C (Figs. 6a–c). However, cation ordering appears to occur rapidly after heating for two additional hours at 1000°C (Fig. 6d). Similar results were obtained for the partially ordered grains examined in this study (Fig. 7), although the intensity profiles suggest that they may have experienced a slight increase in cation order at 750°C and
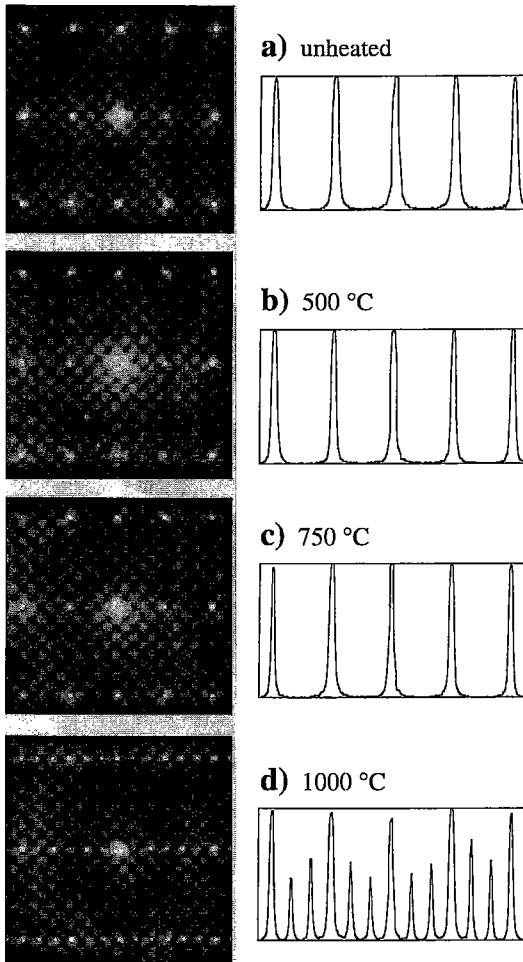
FIG. 6. Electron-diffraction patterns and (h02) intensity profiles of a representative grain of disordered columbite – tantalite before (a) and after heating *in situ* in the electron microscope at 500°C (b), 750°C (c), and 1000°C (d). All experiments carried out for 2 hours at each temperature. [010] zone axis.
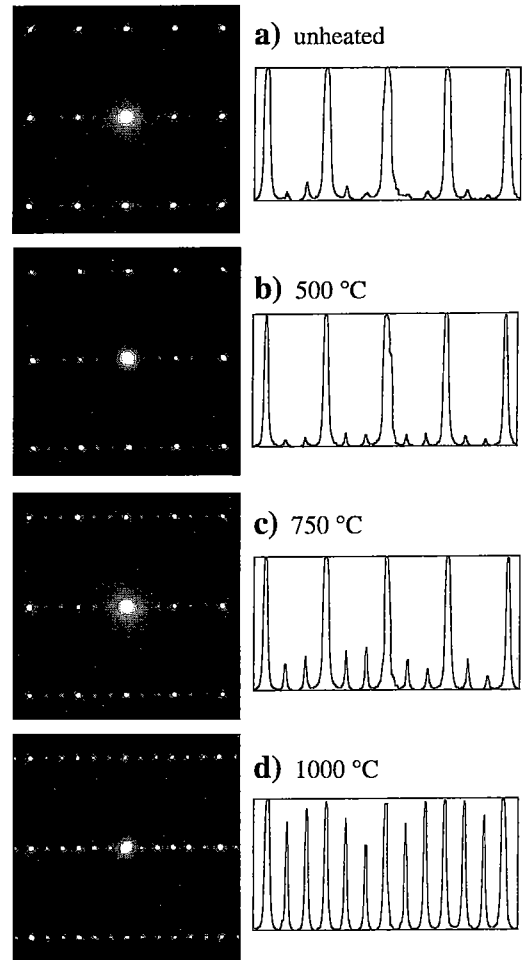

FIG. 7. Electron-diffraction patterns and (h02) intensity profiles of a representative grain of partially ordered columbite – tantalite before (a) and after heating *in situ* in the electron microscope at 500°C (b), 750°C (c), and 1000°C (d). All experiments carried out for 2 hours at each temperature. [010] zone axis.

attained a higher overall degree of order at 1000°C (Figs. 7c, d). These results are consistent with previous heating experiments on bulk samples (*e.g.*, Ercit *et al.* 1995).

Radiation-damage effects

Results of the electron-microprobe analyses indicate average contents of <0.5 wt.% UO_2 for 23 of the 25 samples used in this study. The individual analyses demonstrate, however, that the distribution of U is

inhomogeneous, a feature documented in a previous AEM study of columbite – tantalite from Western Australia (Lumpkin 1992). On the basis of XRD and HRTEM results, all of the Harding samples are highly crystalline and show little evidence of radiation damage. AEM analyses of these regions revealed maximum U contents of 0.2 wt.% UO_2, corresponding to a maximum alpha-decay dose of 8×10^{15} α/mg, a value that is very close to the saturation dose for alpha-decay damage and indicates that the samples should be heavily damaged. However, using the annealing
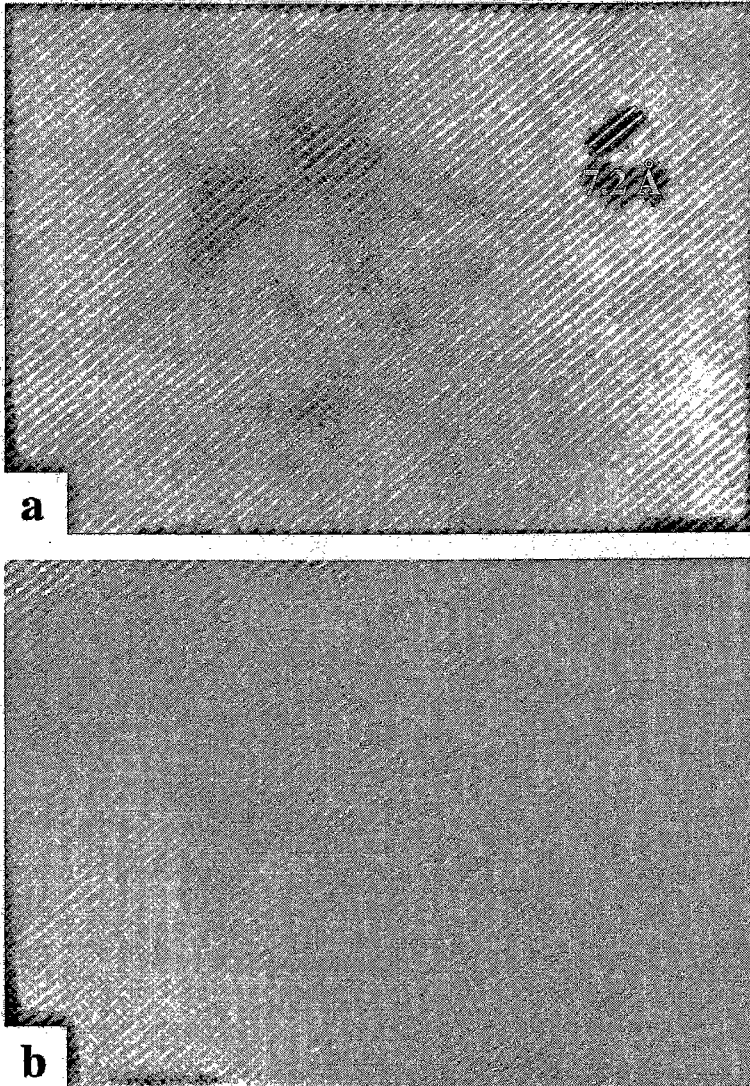
FIG. 8. HRTEM images of radiation damage in two different areas of a grain of columbite
– tantalite from the Harding pegmatite. a) UO_2 = 0.2 wt.%, dose = 8 × 10^{15} α/mg
(1 × 10^{15} α/mg after correction for annealing). b) UO_2 = 0.6 wt.%, dose = 24 × 10^{15} α/mg
(3 × 10^{15} α/mg after correction for annealing). [010] zone axis.

constant of τ_a = 2 × 10^8 years estimated by Lumpkin (1992), a much lower corrected dose of approximately 1 × 10^{15} α/mg is calculated and is consistent with the XRD and HRTEM results.

A few regions having higher U contents, 0.4–0.8 wt.% UO_2, were identified by AEM analysis. Figure 8 shows HRTEM images of two different areas of the same crystal: one of these areas has a U content of 0.2 wt.% UO_2 (8 × 10^{15} α/mg, 1 × 10^{15} α/mg after correction

for annealing), and exhibits nearly continuous lattice-fringes and weak mottled diffraction-contrast (Fig. 8a). The second area has a higher U content, 0.6 wt.% UO_2 (24 × 10^{15} α/mg, 3 × 10^{15} α/mg after correction for annealing), and shows extensive disruption of lattice fringes (Fig. 8b). Radiation-damage domains shown in Figure 8b are in the size range appropriate for isolated alpha-recoil collision cascades (*cf.* Lumpkin & Ewing 1988, Lumpkin *et al.* 1991, Lumpkin 1992), and the

overall microstructure is consistent with the higher U content and corrected dose. Areas of higher U content have not been investigated by HRTEM, but some local regions with U contents of up to 1.5 wt.% UO_2 have been observed in other samples of Harding columbite using optical microscopy and are weakly anisotropic, indicating that some crystallinity may persist at corrected levels of dose as high as 8×10^{15} α/mg (unpubl. data).

DISCUSSION

Columbite – tantalite: composition and fractionation trend

Previous investigations have shown that the level of chemical differentiation attained by a magma responsible for a granitic pegmatite is reflected not only by the assemblage of accessory minerals, but also by the compositions of some of the more common accessory minerals (Černý & Ercit 1985, 1989, Černý 1989a, b). Columbite – tantalite is important in this regard, as it is a major Nb–Ta oxide phase, occurring across the spectrum of pegmatite types in the rare-element class, but particularly in beryl – columbite, complex-spodumene, and complex-lepidolite subtypes (Černý 1989a, b). This sequence of pegmatite subtypes exhibits increasing fractionation in the levels of Li, Rb, Cs, Hf, Ta, F, and B present and in the characteristic Nb–Ta oxide mineral assemblage. In general, the Nb–Ta oxide mineral assemblage changes from columbite – tantalite + ixiolite to columbite – tantalite + microlite + ixiolite + cassiterite + wodginite to microlite + manganocolumbite with increasing fractionation. The latter assemblage is characteristic of the Harding pegmatite. Although the Harding pegmatite is classified as a complex-spodumene pegmatite (Černý 1989a), it is notably poor in Sn and thus lacks cassiterite, wodginite, and ixiolite. As shown by this work, the columbite – tantalite generally contains less than 0.1 wt.% SnO_2. Previous work also shows that microlite usually contains less than 0.1 wt.% SnO_2 (Lumpkin *et al.* 1986). The pegmatite also has several characteristics akin to the complex-lepidolite subtype, including the presence of lepidolite and the dominance of microlite over columbite – tantalite.

In the Harding pegmatite, the columbite – tantalite compositions closely resemble those from the Tanco pegmatite, the Silverleaf offshoot from the Greer Lake pegmatitic granite, and complex pegmatites in the Yellowknife pegmatite field, supporting the idea that a high activity of F promotes effective enrichment in Mn (Černý & Ercit 1985, Černý *et al.* 1986, Černý 1989a). If this holds true, then the limited compositional range of columbite – tantalite from the Harding pegmatite suggests that the activity of F reached a relatively high level prior to final emplacement of the pegmatite and changed very little during the period of crystallization of columbite – tantalite. However, the activity of F does

appear to have increased, as indicated by 1) the appearance of microlite as the dominant Nb–Ta oxide in the interior lithologic units, and 2) the crystallization of late magmatic – hydrothermal lithian muscovite and lepidolite. Subsolidus fluids were probably F-poor as indicated by the low F-content (Heinrich & Levinson 1953, unpubl. data of the author) of rose muscovite in replacement units. In certain Li-rich pegmatites, the composition of columbite – tantalite evolved extensively from ferrocolumbite to manganotantalite, suggesting that the activity of F increased substantially during crystallization (Spilde & Shearer 1992, Černý & Němec 1995).

A better understanding of the enrichment of Mn in columbite – tantalite will require 1) a careful analysis of changes in the activity of F and other components using reliable internal monitors such as apatite, amblygonite – montebrasite, and Li-poor muscovite, 2) an assessment of the partitioning of Mn and Fe into other mineral phases, including garnet, muscovite, and tourmaline, 3) consideration of the bulk composition of the pegmatite in terms of Mn/Fe and Ta/Nb, and 4) experimental work on the crystallization of Nb–Ta oxides in granitic systems. Some progress has been made in the latter area; Linnen (1996) has reported that fractionation of manganocolumbite – manganotantalite in peraluminous melts will result in an increase in Ta/Nb of the melt. Similar experiments need to be carried out including Fe in the system.

Structural state of columbite – tantalite

Effect of cooling rate. The Harding samples are ideal for the study of cation ordering because of the narrow range of Mn/(Mn + Fe) ratios, relatively low Ti contents, and virtual absence of Sn and Sc. The wide range of cation ordering observed in columbite – tantalite from the Harding pegmatite closely resembles the patterns exhibited by the Tanco pegmatite and Silverleaf offshoot from the Greer Lake pegmatitic granite. In their study of the Greer Lake pegmatitic granite and related pegmatites, Černý *et al.* (1986) suggested that columbite – tantalite crystallized initially in the disordered state, and that further ordering was related to the cooling rate of the different igneous bodies. The highest levels of cation order were attained by samples from the pegmatitic granite and its fractionated pods (*f* from about 0.4 to 0.8), with the lowest levels from the outlying pegmatites (*f* from 0 to 0.1), which also contain ixiolite. Columbite – tantalite from the Silverleaf offshoot developed the widest range in degree of order, with a hint of bimodal distribution (*f* from 0 to 0.3 and from 0.5 to 0.7). These results are at least qualitatively consistent with more rapid cooling in the smaller bodies of granitic pegmatites.

The wide range in degree of order and bimodal character (*f* from 0 to 0.4 and from 0.7 to 0.9) of columbite – tantalite from the Tanco pegmatite is also

notable. Ercit (1986) has suggested that the degree of order is related to differences in the rate of crystallization between outer and inner units, with the interior units crystallizing more slowly. In the case of the Harding pegmatite, Chakoumakos & Lumpkin (1990) have approximated the cooling history using a mathematical model involving a number of parameters, including the physical dimensions of the pegmatite, depth, initial temperature of the magma, and host-rock temperature at the time of emplacement. The general form of the cooling curves are similar and indicate that cooling rates may have decreased by as much as 2–3 orders of magnitude during crystallization of the Harding pegmatite, thus supporting the earlier suggestions of Černý et al. (1986) and Ercit (1986). Simulations of this type also suggest that early-formed, disordered columbite – tantalite must pass through a kinetic barrier for cation ordering whereby the extended period of annealing at lower temperature is insufficient to cause further ordering. This is qualitatively consistent with results of the heating experiments carried out in this investigation and in many previous studies (Černý & Ercit, 1985, 1989, Ercit et al. 1995).

Recent experimental work has demonstrated that the partitioning of trace elements between melt and crystals under conditions of rapid crystal-growth in granitic pegmatites can be strongly influenced by the transport properties of the melt (Mungall et al. 1996). However, such an interpretation may be complicated by the influence of a fluid phase on diffusion rates at the crystal – melt interface. Generally, it has been assumed that evolved pegmatite-forming granitic melts are initially saturated in the aqueous fluid component, which begins to exsolve upon commencement of crystallization and assists in element diffusion and the development of giant crystal textures (Jahns & Burnham 1969). This model has been questioned in recent years (London 1987), forcing a reconsideration of the timing of saturation in an aqueous fluid. An important consequence of aqueous fluid undersaturation that may influence cation ordering in columbite – tantalite is an increase in the liquidus temperature, resulting in a modification of the cooling history for a pegmatite of given size and host-rock temperature.

Effect of minor elements. Černý et al. (1986) also noted a possible relationship between the amounts of minor elements and the degree of order in columbite – tantalite from Greer Lake. The amounts of Ti and Sn are all higher in the more disordered samples of columbite, and particularly so in ixiolite. This relationship is also found in the results of the present investigation, where elevated amounts of Ti (0.01 to 0.06 *apfu*, atoms per formula unit) were found in partially ordered and highly disordered specimens. Most of the Ti in these specimens probably occurs in the form of a rutile-like component, $TiTi_2O_6$. A

brannerite-like component, UTi_2O_6, may also account for a small proportion of the Ti in samples from the beryl zone. The Ti content is generally much lower (<0.01 *apfu*) in the highly ordered columbite – tantalite samples from the interior units and may be incorporated as a euxenite-like component, $REETiNbO_6$. Giese (1975) has shown that there are 495 ways to distribute 4 Mn and 8 Nb atoms over the 12 octahedral sites in the unit cell of ordered columbite and that the electrostatic energies of many of these arrangements are close to those of the ideal ordered arrangement with all Mn on 4c and all Nb on 8d. His calculations provide a possible explanation for the common occurrence of disordered structures in nature and suggest that cation ordering may be sensitive to the prevailing physical conditions and the presence of minor elements, provided that the electrostatic energies of the various cation arrangements remain close to those of the ideal ordered arrangement.

It is possible that the negative correlation between minor elements and the degree of cation order is a fortuitous consequence of the geochemical fractionation trend. This is supported by recent evidence of highly ordered columbite – tantalite with elevated minor element contents in the pegmatites of the Bergell intrusion, on the Swiss–Italian border (Wenger & Armbruster 1991). These samples contain 0 to 0.02 *apfu* W, 0.03 to 0.12 *apfu* Ti, and 0 to 0.01 *apfu* Sn, but have order parameters of f between 0.81 and 1.00 and Q between 0.88 and 0.95. Another study of the chemistry and structural state of columbite – tantalite from the Rutherford #2 pegmatite, Amelia County, Virginia (Lumpkin 1998) provides further evidence. The Rutherford #2 samples studied by XRD contain substantial amounts of minor elements including 0 to 0.02 *apfu* W, 0.02 to 0.08 *apfu* Ti, 0 to 0.01 *apfu* Sn, and 0 to 0.01 *apfu REE*, and have relatively ordered distributions of cations (f between 0.73 and 1.00 and Q between 0.79 and 0.98).

Finally, the recent compilation of data presented by Ercit et al. (1995) indicates that numerous partially ordered samples ($0.1 < Q < 0.8$) exist that contain concentrations of the minor elements Ti + Sc + Sn less than 0.05 *apfu*. Furthermore, of the four completely disordered samples in the data set, three have minor element contents of 0.04 to 0.06 *apfu* (Ercit et al. 1995, Fig. 5). The weight of evidence presented here suggests that the major controls of cation order in columbite – tantalite lie in the physical conditions that prevail during crystallization, and that columbite – tantalite might be used as a cooling rate speedometer. The effect of minor elements on cation ordering is unclear, and it is possible that different impurities will result in different cation distributions. Whether or not columbite – tantalite is useful as an indicator of cooling rate can only be determined by an experimental determination of the kinetics of cation ordering.

Radiation-damage effects

Owing to the strong partition of U into microlite and thorite in the Harding pegmatite, most of the columbite – tantalite crystals from the Harding pegmatite have low U contents and are highly crystalline. Radiation damage defined by HRTEM is usually below the level characteristic of the onset of the transformation from crystalline to metamict states in most of the samples. In minerals with ages of 100 Ma or less, this transformation typically occurs over a relatively narrow range of dose, ~0.1 to 1.0×10^{16} α/mg, and is identified in the early stages by mottled diffraction-contrast and isolated-damage cascades. The completely metamict state occurs at a dose of ~1.0×10^{16} α/mg in geologically young samples of pyrochlore and zircon, which is consistent with accelerated damage testing on synthetic phases (Lumpkin & Ewing 1988, Ewing *et al.* 1988). For minerals older than approximately 100 Ma, higher transformation doses have been reported and modeled on the basis of long-term annealing of alpha-recoil collision cascades back to the original crystalline structure.

Calculated doses for the Harding columbite – tantalite samples are generally several times higher than the observed microstructure would indicate. Interpretation of the available data in terms of annealing is consistent with a mean alpha-recoil cascade life, τ_a, of ~2×10^8 years. A similar interpretation can be made using the optical microscope observation that high U-zones are weakly anisotropic and thus retain some crystallinity. Unfortunately, the limited range and inhomogeneous distribution of U contents in columbite – tantalite from the Harding pegmatite preclude a more rigorous determination of radiation-damage ingrowth and the annealing parameter. However, the available results are within the range of estimates for pyrochlore, zircon, and zirconolite, suggesting that long-term annealing of alpha-recoil collision cascades occurs in a variety of structure types in the natural environment.

ACKNOWLEDGEMENTS

REFERENCES

APPLEMAN, D.E. & EVANS, H.T., JR. (1973): Job 9214: indexing and least-squares refinement of powder diffraction data. *U.S. Geol. Surv., Comput. Contrib.* **20** (NTIS Doc. **PB2-16188**).

BENCE, A.E. & ALBEE, A.L. (1968): Empirical correction factors for the electron microanalysis of silicates and oxides. *J. Geol.* **76**, 382-403.

ČERNÝ, P. (1989a): Characteristics of pegmatite deposits of tantalum. *In* Lanthanides, Tantalum and Niobium (P. Möller, P. Černý & F. Saupé, eds.). Springer-Verlag, Berlin, Germany (195-239).

_____ (1989b): Exploration strategy and methods for pegmatite deposits of tantalum. In Lanthanides, Tantalum and Niobium (P. Möller, P. Černý & F. Saupé, eds.). Springer-Verlag, Berlin, Germany (274-302).

_____ & ERCIT, T.S. (1985): Some recent advances in the mineralogy and geochemistry of Nb and Ta in rare-element granitic pegmatites. *Bull. Minéral.* **108**, 499-532.

_____ & _____ (1989): Mineralogy of niobium and tantalum: crystal chemical relationships, paragenetic aspects and their economic implications. In Lanthanides, Tantalum and Niobium (P. Möller, P. Černý & F. Saupé, eds.). Springer-Verlag, Berlin, Germany (27-79).

_____, GOAD, B.E., HAWTHORNE, F.C. & CHAPMAN, R. (1986): Fractionation trends of the Nb- and Ta-bearing oxide minerals in the Greer Lake pegmatitic granite and its pegmatite aureole, southeastern Manitoba. *Am. Mineral.* **71**, 501-517.

_____, MEINTZER, R.E. & ANDERSON, A.J. (1985): Extreme fractionation in rare-element granitic pegmatites: selected examples of data and mechanisms. *Can. Mineral.* **23**, 381-421.

_____ & NĚMEC, D. (1995): Pristine vs. contaminated trends in Nb,Ta-oxide minerals of the Jihlava pegmatite district, Czech Republic. *Mineral. Petrol.* **55**, 117-129.

CHAKOUMAKOS, B.C. & LUMPKIN, G.R. (1990): Pressure – temperature constraints on the crystallization of the Harding pegmatite, Taos County, New Mexico. *Can. Mineral.* **28**, 287-298.

ERCIT, T.S. (1986): *The Simpsonite Paragenesis. The Crystal Chemistry and Geochemistry of Extreme Ta Fractionation.* Ph.D. dissertation, Univ. of Manitoba, Winnipeg, Manitoba.

_____, WISE, M.A. & ČERNÝ, P. (1995): Compositional and structural systematics of the columbite group. *Am. Mineral.* **80**, 613-619.

EWING, R.C., CHAKOUMAKOS, B.C., LUMPKIN, G.R., MURAKAMI, T., GREEGOR, R.B. & LYTLE, F.W. (1988): Metamict minerals: natural analogues for radiation

damage effects in ceramic nuclear waste forms. *Nucl. Instrum. Methods Phys. Res.* **B32**, 487-497.

GIESE, R.F., JR. (1975): Electrostatic energy of columbite/ixiolite. *Nature* **256**, 31-32.

HEINRICH, E.W. (1962): Radioactive columbite. *Am. Mineral.* **47**, 1363-1379.

_____ & LEVINSON, A.A. (1953): Studies in the mica group; mineralogy of the rose muscovites. *Am. Mineral.* **38**, 25-49.

JAHNS, R.H. & BURNHAM, C.W. (1969): Experimental studies of pegmatite genesis. I. A model for the derivation and crystallization of granitic pegmatites. *Econ. Geol.* **64**, 843-864.

_____ & EWING, R.C. (1976): The Harding mine, Taos County, New Mexico. *New Mexico Geol. Soc. Guidebook, 27th Field Conf. (Vermejo Park)*, 263-276.

LINNEN, R.L. (1996): Columbite solubility in granitic melts: implications for pegmatite genesis. *Geol. Assoc. Can. – Mineral. Assoc. Can., Program Abstr.* **21**, A57.

LONDON, D. (1987): Internal differentiation of rare-element granitic pegmatites: effects of boron, phosphorus, and fluorine. *Geochim. Cosmochim. Acta* **51**, 403-420.

LUMPKIN, G.R. (1992): Analytical electron microscopy of columbite: a niobium – tantalum oxide mineral with zonal uranium distribution. *J. Nucl. Mater.* **190**, 302-311.

_____ (1998): Rare-element mineralogy and internal evolution of the Rutherford #2 pegmatite, Amelia County, Virginia: a classic locality revisited. *Can. Mineral.* **36**, 339-353.

_____, CHAKOUMAKOS, B.C. & EWING, R.C. (1986): Mineralogy and radiation effects of microlite from the Harding pegmatite, Taos County, New Mexico. *Am. Mineral.* **71**, 569-588.

_____, EBY, R.K. & EWING, R.C. (1991): Alpha-recoil damage in titanite ($CaTiSiO_5$): direct observation and annealing study using high resolution transmission electron microscopy. *J. Mater. Res.* **6**, 560-564.

_____ & EWING, R.C. (1988): Alpha-decay damage in minerals of the pyrochlore group. *Phys. Chem. Minerals* **16**, 2-20.

_____, SMITH, K.L., BLACKFORD, M.G., GIERÉ, R. & WILLIAMS, C.T. (1994): Determination of 25 elements in the complex oxide mineral zirconolite by analytical electron microscopy. *Micron* **25**, 581-587.

MUNGALL, J.E., DINGWELL, D.B. & CHAUSSIDON, M. (1996): Trace element diffusion in synthetic granitic and granitic pegmatite melts. *Geol. Assoc. Can. – Mineral. Assoc. Can., Program Abstr.* **21**, A68.

NICKEL, E.H., ROWLAND, J.F. & McADAM, R.C. (1963): Ixiolite – a columbite substructure. *Am. Mineral.* **48**, 961-979.

SPILDE, M.N. & SHEARER, C.K. (1992): A comparison of tantalum – niobium oxide assemblages in two mineralogically distinct rare-element granitic pegmatites, Black Hills, South Dakota. *Can. Mineral.* **30**, 719-737.

STURDIVANT, J.R. (1930): The crystal structure of columbite. *Z. Kristallogr.* **75**, 88-108.

SUCHOMEL, T.J. (1976): *Geology and Mineralogy of the Harding Pegmatite, Taos County, New Mexico.* M.S. thesis, Univ. of Illinois at Urbana – Champaign, Urbana, Illinois.

VON KNORRING, O. & FADIPE, A. (1981): On the mineralogy and geochemistry of niobium and tantalum in some granite pegmatites and alkali granites of Africa. *Bull. Minéral.* **104**, 496-507.

WENGER, M. & ARMBRUSTER, T. (1991): Columbite (Fe,Mn)(Nb,Ta)$_2$O$_6$ in the pegmatites of the calc-alkaline Bergell intrusion (southeast Central Alps). *Schweiz. Mineral. Petrogr. Mitt.* **71**, 349-369.

WISE, M.A., TURNOCK, A.C. & ČERNÝ, P. (1985): Improved unit cell dimensions for ordered columbite – tantalite end members. *Neues Jarhb. Mineral., Monatsh.*, 372-378.